

Anomalous Dispersion of LO Phonons in Oxygen-Doped $\text{La}_{2-x}\text{Sr}_x\text{CuO}_{4+\delta}$

Tim Tejsner,^{1,2} Andrea Piovano,¹ Ana ȚuȚueanu,^{1,2} Astrid T. Rømer,¹
Barrett O. Wells,³ Jean-Claude Grivel,⁴ Martin Boehm,¹ and Linda Udby²

¹*Institut Laue-Langevin, 71 Avenue des Martyrs, 38000 Grenoble, France*

²*Nanoscience Center, Niels Bohr Institute, University of Copenhagen, DK-2100 Copenhagen, Denmark*

³*Department of Physics, University of Connecticut, Storrs, Connecticut 06269, USA*

⁴*Department of Energy Conversion and Storage, Technical University
of Denmark, Frederiksborgvej 399, DK-4000 Roskilde, Denmark*

(Dated: August 27, 2019)

Inelastic neutron scattering has been used to study the in-plane Cu-O bond-stretching mode in oxygen doped $\text{La}_{2-x}\text{Sr}_x\text{CuO}_{4+\delta}$ ($T_c = 38$ K) and $\text{La}_2\text{CuO}_{4+\delta}$ ($T_c = 43$ K). Similar to results from optimally doped $\text{La}_{1.85}\text{Sr}_{0.15}\text{CuO}_4$ ($T_c = 35$ K), we observe anomalous features in the dispersion of this half-breathing mode in the form of a softening halfway through the Brillouin Zone. Considering the differences in electronic structure and local environment between the oxygen- and strontium-doped compounds with similar T_c , we rule out a connection between the phonon anomaly and structural instabilities related to the specific dopant type. We interpret the phonon anomaly as a signature of correlated charge fluctuations possibly connected to stripes.

A widely accepted description of the low-temperature electronic state of underdoped cuprate superconductors is the ‘stripe’-picture, where, due to hole-doping, the anti-ferromagnetic (AFM) ground state of the parent compound is segregated by channels of charge resulting in magnetic anti-phase boundaries [1]. Experimentally, the magnetic part of the stripes shows up in neutron scattering experiments as a modulated AFM structure (static magnetic stripes) and excitations emerging with similar wavevectors, in the low energy regime (dynamic magnetic stripes).

While experimental evidence of magnetic stripes have been extensively documented (see e.g. [2] for a review), the charge component of the stripes is more elusive. Static charge stripes only show up in superconducting (SC) samples close to the $x = \frac{1}{8}$ anomaly [1, 3–6] and direct evidence of dynamic charge stripes has only been reported for isostructural, but insulating $\text{La}_{2-x}\text{Sr}_x\text{NiO}_4$ [7]. Understanding the relationship between these four signatures of stripe formation as a function of doping would be a crucial leap forward in our understanding of the cuprates.

Since direct, spectroscopic evidence of fluctuating charge stripes in SC cuprates is lacking, it may be possible to find an avenue of progress through indirect measurements. Recently, it was discovered that the dispersion of the Cu-O bond-stretching longitudinal-optical (LO) phonon in SC $\text{La}_{1.85}\text{Sr}_{0.15}\text{CuO}_4$ (LSCO15, $T_c = 38$ K) [8] and $\text{La}_{1.80}\text{Sr}_{0.20}\text{CuO}_4$ ($T_c \approx 35$ K) [9] displays a strong anomalous softening interpreted as a coupling to a novel charge collective mode [9]. Furthermore, merely a weak signature of the anomaly is visible in the phonon linewidth of $\text{La}_{1.93}\text{Sr}_{0.07}\text{CuO}_4$ ($T_c \approx 15$ K) and $\text{La}_{1.75}\text{Sr}_{0.25}\text{CuO}_4$ ($T_c \approx 15$ K), suggesting that the strength of the anomaly tracks the doping-dependence of T_c [9].

Similar phonon anomalies have been observed in $\text{Bi}_2\text{Sr}_2\text{CaCu}_2\text{O}_{8+\delta}$ [10], $\text{La}_{1.875}\text{Ba}_{0.125}\text{CuO}_4$ (LBCO) [11], $\text{La}_{1.48}\text{Nd}_{0.4}\text{Sr}_{0.12}\text{CuO}_4$ (LNSCO) [8]

and $\text{YBa}_2\text{Cu}_3\text{O}_{6.6}$ [12] hinting at a ubiquitous feature of cuprate superconductors.

In order to further investigate the robustness of the phonon anomaly in the $0.1 < x < 0.2$ doping range, we examine two compounds derived from La_2CuO_4 with unique magnetic, structural and superconducting properties.

Hole-doping of the parent compound La_2CuO_4 can be performed by introducing two distinct dopant species. Replacing La^{3+} for Sr^{2+} yields $\text{La}_{2-x}\text{Sr}_x\text{CuO}_4$ (LSCO) with ‘quenched doping’ [13], meaning that Sr has a fixed random distribution on La sites after crystal growth. On the other hand, an ‘annealed doping’ [13] can be obtained by introducing excess, mobile oxygen anions into the lattice by electrochemical methods [14], obtaining $\text{La}_2\text{CuO}_{4+\delta}$ (LCO+O). At low Sr concentrations ($x \leq 0.14$) it is possible to combine Sr and O dopants, resulting in ‘co-doped’ $\text{La}_{2-x}\text{Sr}_x\text{CuO}_{4+\delta}$ (LSCO+O) [15]. Fig. 1A depicts the crystallographic sites of O/Sr dopant ions [16–18].

Quenched Sr^{2+} doping creates a superconductor where T_c varies continuously with doping, forming the so-called superconducting dome for $0.05 \leq x \leq 0.25$. Meanwhile the mobile O dopants only seem to allow for certain superconducting phases to emerge ($T_c = 16, 32, \approx 40$ K) due to oxygen content [19], pressure [20] or thermal treatment [21].

At sufficient O-doping, LSCO+O is superconducting at ambient pressure below $T_c \approx 40$ K, regardless of Sr-content [15]. While the underlying mechanism for the connection between annealed disorder and superconductivity is far from settled, the distribution of O dopants is clearly distinct from the distribution of Sr^{2+} dopants. Contrary to the quenched Sr^{2+} dopants, annealed O dopants in LSCO+O are responsible for a number of structural ordering phenomena such as staging [22, 23] and fractal-like distributions of ordered superstructure patches [21, 24].

Differences can also be observed in the magnetic struc-

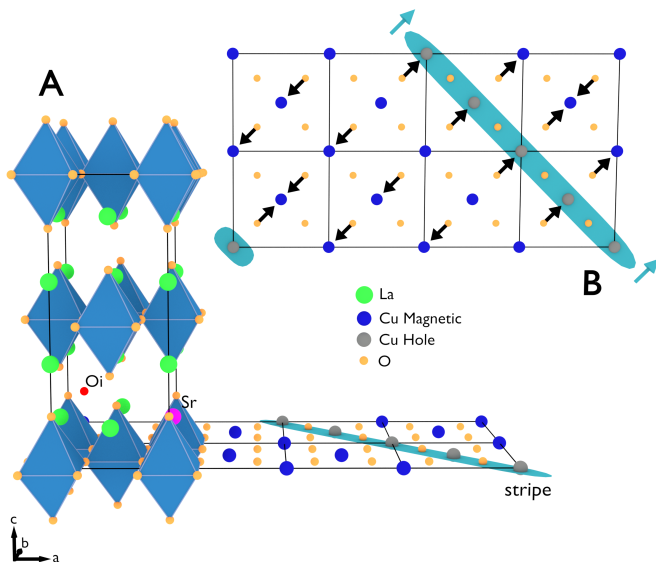


FIG. 1. **A:** Sketch of $\text{La}_{2-x}\text{Sr}_x\text{CuO}_{4+\delta}$ in the orthorhombic unit cell with two distinct dopant species: Sr^{2+} replacing La^{3+} and interstitial oxygen (Oi). The supercell contains 32 formula units, and the two singular dopant species thus represent a doping of $n_h = \frac{3}{32} \approx 0.09$. Blue Cu atoms represent anti-ferromagnetic regions while grey Cu atoms represent a static charge stripe with $\frac{1}{2}$ hole per Cu. **B:** Sketch of in-phase displacement of dynamic charge domain wall modes coupled to the phonon. Black arrows represent the displacement due to the Cu-O half-breathing mode at $\mathbf{q} = (0.25, 0.25, 0)$, while teal arrows represent the in-phase phason mode of the charge stripe [25].

ture of the two compounds. In LSCO+O, the transition to static magnetic stripe order, T_N , roughly coincides with T_c [26]. In LSCO, on the other hand, it generally holds that the spins freeze gradually with decreasing temperature and $T_N < T_c$ up to a doping of $x = 0.13$, above which the magnetic spectrum becomes gapped [27, 28]. This difference in magnetic signatures can partially be explained by the fact that LSCO+O phase separates into distinct spin-stripe ordered ($x \approx \frac{1}{8}$) and optimally superconducting ($x \approx 0.16$) phases, regardless of strontium content prior to oxygenation [15, 26].

In this Letter, we investigate the effects of oxygen disorder on the Cu-O bond-stretching phonon mode by providing evidence of phonon anomalies in oxygen-doped LCO+O and co-doped $\text{La}_{1.94}\text{Sr}_{0.06}\text{CuO}_{4.035}$ (LSCO6+O). If the phonon anomaly is related to a specific structural instability due to quenched disorder, one would expect a different response of the lattice in oxygen-doped compounds with annealed disorder. Our results show remarkable similarities of the phonon anomaly in LCO+O, LSCO+O and LSCO. This points towards a purely electronic origin of the phonon anomaly. In order to investigate the possible connection to static stripe order, we explore the effects of a 10 T applied magnetic field. A 10 T field is known to significantly increase the static magnetic response for both LCO+O [29]

and LSCO6+O [30]. The presence of a field-induced enhancement of the phonon anomaly would indicate a direct connection to static magnetic stripe order, while the absence of a field-effect would point to another source of the anomaly. We observe no detectable change in the phonon signal with applied field, an observation which is compatible with the phonon coupling to *dynamic* charge fluctuations as has been suggested previously [11]. Our observations thus reinforce and expand this interpretation more broadly for doped cuprates.

The samples are high quality LCO+O and LSCO6+O single crystals. The oxygen-stoichiometric samples were grown by the Traveling Solvent Float Zone method. Subsequently, oxygen intercalation was performed using wet-chemical methods [14]. Both samples are optimally superconducting with $T_c = 43$ K (LCO+O) and $T_c = 37.5$ K (LSCO6+O), confirmed by magnetization measurements (See Fig. S1 in Supplemental Material (SM)). Prior to oxygen intercalation the samples were insulating (LCO) or had $T_c = 8$ K (LSCO6).

Throughout this Letter, all Miller indices are described with reference to the orthorhombic Bmab space group and the samples are aligned in the a - b plane. Lattice parameters were found to be $a = b \approx 5.35(5)$ Å, $c \approx 13.1(1)$ Å for both samples.

Neutron scattering experiments were performed on the IN8 thermal Triple-Axis Spectrometer at Institut Laue-Langevin, Grenoble [31, 32]. The instrument was configured with a silicon (311) monochromator and pyrolytic graphite (002) analyser in order to access the desired dynamical range while obtaining the best compromise between neutron intensity and energy resolution (≈ 4 -5 meV at 80 meV energy transfer with final wavevector $k_f = 2.226$ Å⁻¹). We made use of a position sensitive detector (PSD) with a horizontal spatial resolution of 5 mm in order to identify and subtract spurious scattering (see Fig. S3 and S4 in SM).

Figure 2 shows the reduced data at selected wavevectors for both LSCO6+O and LCO+O. The data has been fitted to a Damped Harmonic Oscillator (DHO) model [33] with a flat background, convoluted with instrument resolution:

$$S(\mathbf{q}, \omega) = I_{\text{ph}} \frac{1}{\pi \omega_{\mathbf{q}}} \frac{\gamma}{(\omega - \omega_{\mathbf{q}})^2 + \gamma^2} + I_{\text{BG}},$$

where I_{ph} is the phonon intensity, $\omega_{\mathbf{q}}$ the phonon energy at wave vector \mathbf{q} , γ the phonon linewidth and I_{BG} the background intensity.

The extracted dispersion from the zero-field data is shown in Fig. 3 along with a normal sinusoidal dispersion, $\hbar\omega_{\mathbf{q}} = \alpha \cos(2\pi\mathbf{q}) + \beta$, inferred from phonon calculations on LSCO using Density Functional Theory (See Fig. S5 in SM and [34]). We fit the cosine-function to points near the zone center ($\mathbf{q} = (0, 0, 0)$) and edge ($\mathbf{q} = (\frac{1}{2}, \frac{1}{2}, 0)$) to obtain the dashed curves of Fig. 3A. To quantify the magnitude of the anomaly, we define the

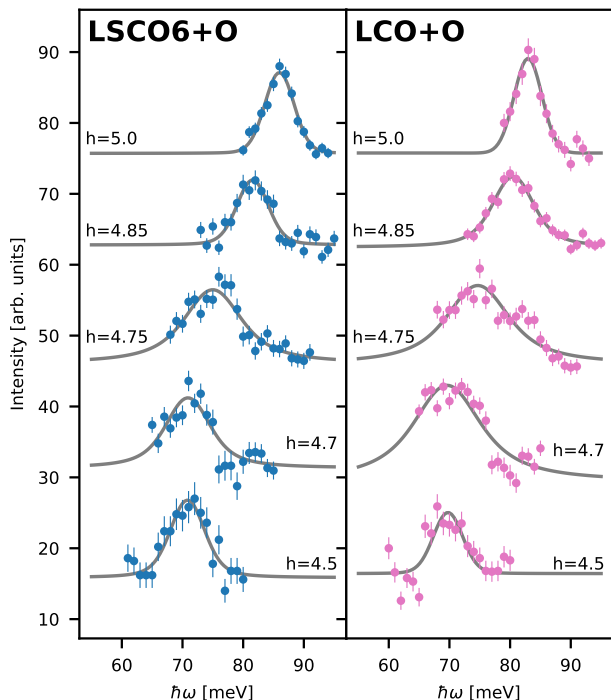


FIG. 2. Reduced data at selected wavevectors of the form $Q = (h, h, 0)$ for both LSCO6+O and LCO+O at $T = 5$ K and $H = 0$ T. Data at $Q = (5, 5, 0)$ and $Q = (4.85, 4.85, 0)$ was scaled by a factor of $\frac{1}{2}$ for clarity due to an increase of intensity from the phonon form factor. Data at different h are offset for clarity. Solid lines are fits to a DHO lineshape (see text).

‘anomaly signal’ as the difference between the normal dispersion and the measured data (gray shaded area in Fig. 3A). Fig. 3B shows our anomaly signal for LCO+O and LSCO6+O along with previous results from optimally doped LSCO15 and insulating, stripe-ordered LNSCO [8]. We emphasize the presence of similar anomaly signals on an absolute scale across all studied samples. The linewidth broadening γ follows the softening of $\omega_{\mathbf{q}}$ similar to what was observed in LSCO15 and LNSCO [8] (see Fig. S2 in SM). Finally, our data can be qualitatively described by a linear combination of stripe ordered and optimally superconducting anomaly signals (See Fig. S7 in SM), consistent with the observation of phase separation in the (super)oxygenated compounds [15].

To begin the discussion of our results, we remark that softening and/or broadening of phonon modes is generally a signature of an incipient structural or electronic instability. Typical examples include structural phase transitions, \mathbf{q} -dependence of the electron-phonon matrix element, Fermi surface nesting and electronic correlations [35]. In order to determine the origin of a given phonon anomaly, it is therefore important to carefully exhaust alternatives before making statements about the connection to novel phases such as dynamic charge stripes.

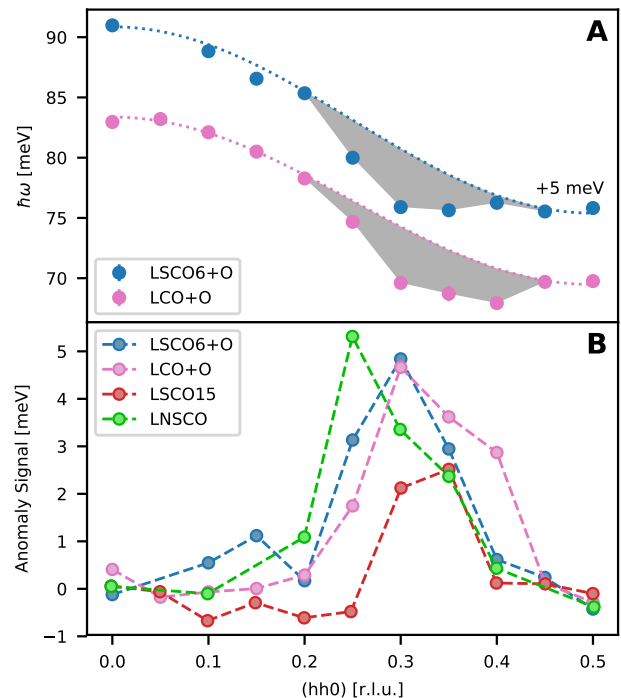


FIG. 3. (A): Dispersion of the LO phonon obtained from the peak positions of individual spectra of both LCO+O and LSCO6+O (offset by 5 meV for clarity). Error bars smaller than the markers are not shown. Dashed line is the normal sinusoidal dispersion as described in the text. All data was obtained at $T = 5$ K. (B): Difference between sinusoidal and measured dispersion in $\text{La}_2\text{CuO}_{4+\delta}$ (LCO+O) $\text{La}_{2-x}\text{Sr}_x\text{CuO}_{4+\delta}$ (LSCO+O), $\text{La}_{1.85}\text{Sr}_{0.15}\text{CuO}_4$ (LSCO15) and $\text{La}_{1.48}\text{Nd}_{0.4}\text{Sr}_{0.12}\text{CuO}_4$ (LNSCO). Data for LSCO15 and LNSCO adapted from [8].

The phonon anomaly appears in vicinity of the wave vector $\mathbf{q}_{\text{cp}} = (\frac{1}{4}, \frac{1}{4}, 0)$, consistent with charge stripe ordering as illustrated in Fig. 1. Measurements of LNSCO [36], LSCO15 [8] and LBCO [8] have shown a suppression of the anomaly as one moves away from the bond-stretching direction [36], supporting a one dimensional stripe-like picture. Since static stripe order has, so far, not been observed in LSCO15 any connection between the phonon anomaly and stripes is likely dynamic. Additionally, the phonon anomaly in LSCO15 and LBCO has almost no temperature dependence apart from a slightly sharper peak shape when heating from 10 K to 300 K [8, 11]. These phenomena rule out anharmonicity and structural inhomogeneity as mechanisms for the phonon anomaly in these systems.

A combination of inelastic X-ray and ARPES measurements on overdoped LSCO ($x = 0.2$ and $x = 0.3$) have shown that the phonon anomaly wavevector is inconsistent with Fermi surface nesting [9, 37], contradicting the idea of a phonon softening due to a Kohn anomaly. A different, possibly \mathbf{q} -dependent, electron-phonon coupling could still be responsible for the phonon anomaly. Such

an effect would renormalize the electronic quasiparticle dispersion (the so-called ‘ARPES kink’ [38]) at energies similar to the phonon softening. The ARPES kink has been observed in LSCO $x = 0.2$ and $x = 0.3$, but since only LSCO $x = 0.2$ shows anomalous phonons, the two phenomena appear to not be connected [9].

Thus, all previous studies are unable to explain the phonon anomaly through conventional means and any coupling to stripe order is likely dynamic. One possible scenario is a coupling of the Cu-O bond-stretching phonon with steeply dispersing charge fluctuations. Kaneshita *et al.* performed calculations based on the Hubbard model of this scenario, predicting anomalous phonon dispersions due to both transverse (meandering) and longitudinal (compression) coherent stripe fluctuations [25] (see Fig. 1 for a sketch of the transverse mode). We emphasize that the observed phonon anomaly reported here (see Fig. 3) and in LBCO/LSCO [8, 11] is remarkably similar to the prediction of Kaneshita *et al.* (see Fig. 5 in [25]).

Despite differences in the magnetic excitation spectra as recorded by neutron scattering (including low and zero energy transfers), the three materials LCO+O, LSCO6+O and LSCO15 have remarkably similar in-plane Cu-O bond-stretching dispersions (Fig. 3). Furthermore, static charge order at zero field has been observed in a different sample of LCO+O [39] and in LNSCO [3] but so far not in LSCO6+O nor in LSCO15. These observations together rule out a unique, direct connection between static stripes (spin and charge) and the phonon anomaly. In order to further confirm this point, we performed scans of LSCO6+O at selected wave vectors in a $H = 10$ T magnetic field which is known to induce a considerable volume of stripe-like magnetic order in this particular sample [30]. While static charge order has not been observed in LSCO6+O, measurements on LSCO ($x = 0.12$) have shown that static charge and spin stripes respond identically to magnetic fields [4].

Figure 4 contains data at two wave vectors with and without an applied magnetic field of 10 T, clearly showing the absence of any detectable field effect on the in-plane Cu-O bond-stretching phonon at $\mathbf{q} = (\frac{1}{4}, \frac{1}{4}, 0)$. These measurements were performed simultaneously with measurements of the low-energy magnetic fluctuations [40], confirming a significant increase in the magnetic spectral weight towards lower energies consistent with the appearance of field-induced stripe-order [30]. Thus, the appearance of static magnetic stripe order does not affect the phonon anomaly in LSCO6+O. A similar insensitivity of the phonon anomaly to an applied magnetic field has been observed in underdoped ($T_c = 66$ K) YBa₂CuO_{6.6} [41].

We have shown that the phonon anomaly is a robust feature in optimally doped as well as stripe-ordered cuprates which is independent of the structural details related to the doping process. Since it is equally well-formed in stripe-ordered and optimally doped systems, where the latter show no static magnetic order, the

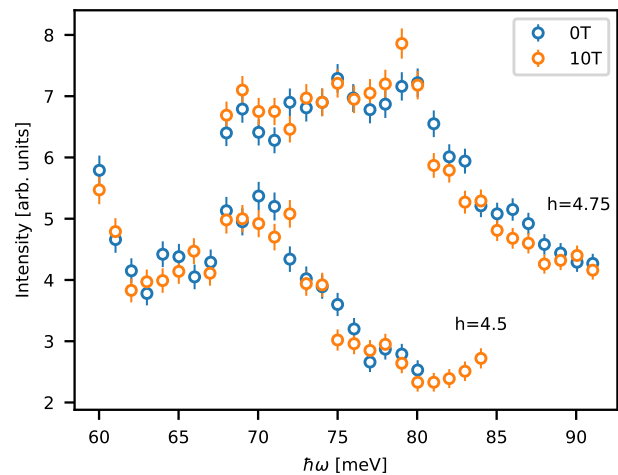


FIG. 4. Comparison of representative constant- Q ($h, h, 0$) scans of La_{1.94}Sr_{0.06}CuO_{4.035} in zero-field and with an applied field of 10 T. All measurements performed at $T = 5$ K

anomaly is surprisingly insensitive to low-energy magnetic characteristics. This is further confirmed by the absence of a magnetic field effect in LSCO6+O which introduces static magnetic stripe-order.

The phonon anomaly is strongest in the doping region around optimal T_c ($0.125 \leq n_h \leq 0.20$) (LSCO15, LNSCO [8], LBCO [11], LSCO6+O, LCO+O), regardless of the presence of static charge order (LNSCO [1], LBCO [42]), suppression of bulk superconductivity (LNSCO [3]) or dopant disorder (LCO+O, LSCO6+O). In addition, the phonon anomaly is unaffected by magnetic fields (LSCO6+O, YBa₂CuO_{6.6} [41]) and temperature (LBCO, LSCO15) [8]). Thus it appears to be an intrinsic, robust signature of doped cuprates near optimal doping .

In conclusion, we have measured the in-plane Cu-O bond-stretching phonon in LSCO6+O and LCO+O and provided evidence for significant anomalous behavior. Since one sample (LCO+O) exhibits charge order [39] while the other (LSCO6+O) does not [30], and since the samples also have distinct magnetic spectra with distinct field dependencies [30, 43] we conclude that the phonon anomaly has no direct, trivial relationship to either magnetic or charge static order. In addition, the unique structural characteristics of oxygen-doped samples rule out a connection between the specific dopant species and the phonon anomaly. We proceed to conclude that the phonon anomaly is a signature of transverse charge stripe fluctuations. If fluctuating stripes are the fundamental degrees of freedom relevant for the cuprates, it is appealing to draw a connection to Pair-Density-Wave superconductors [44]. In this system, the fundamental degrees of freedom are transverse charge fluctuations in an ‘electronic liquid crystal’ phase without long range order [45]. In this scenario, the phonon anomaly in materials without static stripe order is due to a matching of the

phonon wavevector with, otherwise undetectable, short-range transverse stripe correlations. The $x = \frac{1}{8}$ anomaly

then corresponds to the special case where stripes exhibit long-range order.

-
- [1] J. M. Tranquada, B. J. Sternlieb, J. D. Axe, Y. Nakamura, and S. Uchida, *Nature* **375**, 561 (1995).
- [2] J. M. Tranquada, *AIP Conference Proceedings* **1550**, 114 (2013).
- [3] J. M. Tranquada, J. D. Axe, N. Ichikawa, Y. Nakamura, S. Uchida, and B. Nachumi, *Phys. Rev. B* **54**, 7489 (1996).
- [4] N. B. Christensen, J. Chang, J. Larsen, M. Fujita, M. Oda, M. Ido, N. Momono, E. M. Forgan, A. T. Holmes, J. Mesot, M. Huecker, and M. v Zimmermann, *arXiv:1404.3192 [cond-mat]* (2014), *arXiv:1404.3192 [cond-mat]*.
- [5] V. Thampy, M. P. M. Dean, N. B. Christensen, L. Steinke, Z. Islam, M. Oda, M. Ido, N. Momono, S. B. Wilkins, and J. P. Hill, *Phys. Rev. B* **90**, 100510 (2014).
- [6] T. P. Croft, C. Lester, M. S. Senn, A. Bombardi, and S. M. Hayden, *Phys. Rev. B* **89**, 224513 (2014).
- [7] S. Anissimova, D. Parshall, G. D. Gu, K. Marty, M. D. Lumsden, S. Chi, J. A. Fernandez-Baca, D. L. Abernathy, D. Lamago, J. M. Tranquada, and D. Reznik, *Nature Communications* **5**, 3467 (2014).
- [8] D. Reznik, L. Pintschovius, M. Fujita, K. Yamada, G. D. Gu, and J. M. Tranquada, *J Low Temp Phys* **147**, 353 (2007).
- [9] S. R. Park, T. Fukuda, A. Hamann, D. Lamago, L. Pintschovius, M. Fujita, K. Yamada, and D. Reznik, *Phys. Rev. B* **89**, 020506 (2014).
- [10] L. Chaix, G. Ghiringhelli, Y. Y. Peng, M. Hashimoto, B. Moritz, K. Kummer, N. B. Brookes, Y. He, S. Chen, S. Ishida, Y. Yoshida, H. Eisaki, M. Salluzzo, L. Braicovich, Z.-X. Shen, T. P. Devereaux, and W.-S. Lee, *Nature Physics* **13**, 952 (2017).
- [11] D. Reznik, L. Pintschovius, M. Ito, S. Iikubo, M. Sato, H. Goka, M. Fujita, K. Yamada, G. D. Gu, and J. M. Tranquada, *Nature* **440**, 1170 (2006).
- [12] M. Le Tacon, A. Bosak, S. M. Souliou, G. Dellea, T. Loew, R. Heid, K.-P. Bohnen, G. Ghiringhelli, M. Krisch, and B. Keimer, *Nature Physics* **10**, 52 (2014).
- [13] B. O. Wells, Y. S. Lee, M. A. Kastner, R. J. Christianson, R. J. Birgeneau, K. Yamada, Y. Endoh, and G. Shirane, *Science* **277**, 1067 (1997).
- [14] P. Blakeslee, R. J. Birgeneau, F. C. Chou, R. Christianson, M. A. Kastner, Y. S. Lee, and B. O. Wells, *Phys. Rev. B* **57**, 13915 (1998).
- [15] H. E. Mohottala, B. O. Wells, J. I. Budnick, W. A. Hines, C. Niedermayer, L. Udby, C. Bernhard, A. R. Moodenbaugh, and F.-C. Chou, *Nature Materials* **5**, 377 (2006).
- [16] P. G. Radaelli, D. G. Hinks, A. W. Mitchell, B. A. Hunter, J. L. Wagner, B. Dabrowski, K. G. Vandervoort, H. K. Viswanathan, and J. D. Jorgensen, *Phys. Rev. B* **49**, 4163 (1994).
- [17] C. Rial, E. Morán, M. A. Alario-Franco, U. Amador, and N. H. Andersen, *Physica C: Superconductivity* **254**, 233 (1995).
- [18] C. Rial, E. Morán, M. A. Alario-Franco, U. Amador, and N. H. Andersen, *Physica C: Superconductivity* **278**, 122 (1997).
- [19] L. H. Liu, G. C. Che, J. Zhao, and Z. X. Zhao, *Physica C: Superconductivity* **425**, 37 (2005).
- [20] B. Lorenz, Z. G. Li, T. Honma, and P.-H. Hor, *Phys. Rev. B* **65**, 144522 (2002).
- [21] M. Fratini, N. Poccia, A. Ricci, G. Campi, M. Burghammer, G. Aeppli, and A. Bianconi, *Nature* **466**, 841 (2010).
- [22] B. O. Wells, R. J. Birgeneau, F. C. Chou, Y. Endoh, D. C. Johnston, M. A. Kastner, Y. S. Lee, G. Shirane, J. M. Tranquada, and K. Yamada, *Zeitschrift für Physik B Condensed Matter* **100**, 535 (1996).
- [23] P. J. Ray, N. H. Andersen, T. B. S. Jensen, H. E. Mohottala, C. Niedermayer, K. Lefmann, B. O. Wells, M. v Zimmermann, and L. Udby, *Phys. Rev. B* **96**, 174106 (2017).
- [24] N. Poccia, A. Ricci, G. Campi, M. Fratini, A. Puri, D. D. Gioacchino, A. Marcelli, M. Reynolds, M. Burghammer, N. L. Saini, G. Aeppli, and A. Bianconi, *PNAS* **109**, 15685 (2012).
- [25] E. Kaneshita, M. Ichioka, and K. Machida, *Phys. Rev. Lett.* **88**, 115501 (2002).
- [26] L. Udby, J. Larsen, N. B. Christensen, M. Boehm, C. Niedermayer, H. E. Mohottala, T. B. S. Jensen, R. Toft-Petersen, F. C. Chou, N. H. Andersen, K. Lefmann, and B. O. Wells, *Phys. Rev. Lett.* **111**, 227001 (2013).
- [27] K. Hirota, *Physica C: Superconductivity* **357-360**, 61 (2001).
- [28] M. H. Julien, *Physica B: Condensed Matter Proceedings of the 23rd International Conference on Low Temperature Physics*, **329-333**, 693 (2003).
- [29] Y. S. Lee, F. C. Chou, A. Tewary, M. A. Kastner, S. H. Lee, and R. J. Birgeneau, *Phys. Rev. B* **69**, 020502 (2004).
- [30] S. Holm-Dahlin, J. Larsen, H. Jacobsen, A. T. Rømer, A.-E. Tūţeanu, M. Ahmad, J.-C. Grivel, T. Goko, R. Scheuermann, M. v Zimmermann, M. Boehm, P. Steffens, K. Conder, C. Niedermayer, K. S. Pedersen, N. B. Christensen, S. B. Emery, B. O. Wells, K. Lefmann, and L. Udby, *Manuscript in preparation* (2019).
- [31] T. Tejsner, A. Piovano, A.-E. Tūţeanu, M. Boehm, and L. Udby, *Institut Laue-Langevin (ILL)* (2018), doi:10.5291/ILL-DATA.7-01-458.
- [32] T. Tejsner, A. Piovano, A.-E. Tūţeanu, M. Boehm, and L. Udby, *Institut Laue-Langevin (ILL)* (2018), doi:10.5291/ILL-DATA.7-01-474.
- [33] B. Fåk and B. Dorner, *Physica B: Condensed Matter Proceedings of the First European Conference on Neutron Scattering*, **234-236**, 1107 (1997).
- [34] F. Giustino, M. L. Cohen, and S. G. Louie, *Nature* **452**, 975 (2008).
- [35] D. Reznik, *Physica C: Superconductivity Stripes and Electronic Liquid Crystals in Strongly Correlated Materials*, **481**, 75 (2012).
- [36] D. Reznik, T. Fukuda, D. Lamago, A. Q. R. Baron, S. Tsutsui, M. Fujita, and K. Yamada, *Journal of Physics and Chemistry of Solids SNS2007*, **69**, 3103 (2008).
- [37] S. R. Park, Y. Cao, Q. Wang, M. Fujita, K. Yamada,

- S.-K. Mo, D. S. Dessau, and D. Reznik, *Phys. Rev. B* **88**, 220503 (2013).
- [38] D. R. Garcia and A. Lanzara, *Advances in Condensed Matter Physics* **2010** (2010), 10.1155/2010/807412.
- [39] Z. Zhang, R. Sutarto, F. He, F. C. Chou, L. Udby, S. L. Holm, Z. H. Zhu, W. A. Hines, J. I. Budnick, and B. O. Wells, *Phys. Rev. Lett.* **121**, 067602 (2018).
- [40] Manuscript in preparation (2019).
- [41] D. Reznik, D. Parshall, S. R. Park, J. W. Lynn, and T. Wolf, *J Supercond Nov Magn* **29**, 643 (2016).
- [42] M. Fujita, H. Goka, K. Yamada, J. M. Tranquada, and L. P. Regnault, *Phys. Rev. B* **70**, 104517 (2004).
- [43] H. Jacobsen, S. L. Holm, M.-E. Lăcătușu, A. T. Rømer, M. Bertelsen, M. Boehm, R. Toft-Petersen, J.-C. Grivel, S. B. Emery, L. Udby, B. O. Wells, and K. Lefmann, *Phys. Rev. Lett.* **120**, 037003 (2018).
- [44] E. Fradkin, S. A. Kivelson, and J. M. Tranquada, *Rev. Mod. Phys.* **87**, 457 (2015).
- [45] S. A. Kivelson, E. Fradkin, and V. J. Emery, *Nature* **393**, 550 (1998).

Supplemental Material for: Anomalous Dispersion of LO Phonons in Oxygen-Doped $\text{La}_{2-x}\text{Sr}_x\text{CuO}_{4+\delta}$

Tim Tejsner,^{1,2} Andrea Piovano,¹ Ana ȚuȚueanu,^{1,2} Astrid T. Rømer,¹
Barrett O. Wells,³ Jean-Claude Grivel,⁴ Martin Boehm,¹ and Linda Udby²

¹*Institut Laue-Langevin, 71 Avenue des Martyrs, 38000 Grenoble, France*

²*Nanoscience Center, Niels Bohr Institute, University of Copenhagen, DK-2100 Copenhagen, Denmark*

³*Department of Physics, University of Connecticut, Storrs, Connecticut 06269, USA*

⁴*Department of Energy Conversion and Storage, Technical University of Denmark, Frederiksborgvej 399, DK-4000 Roskilde, Denmark*

(Dated: August 27, 2019)

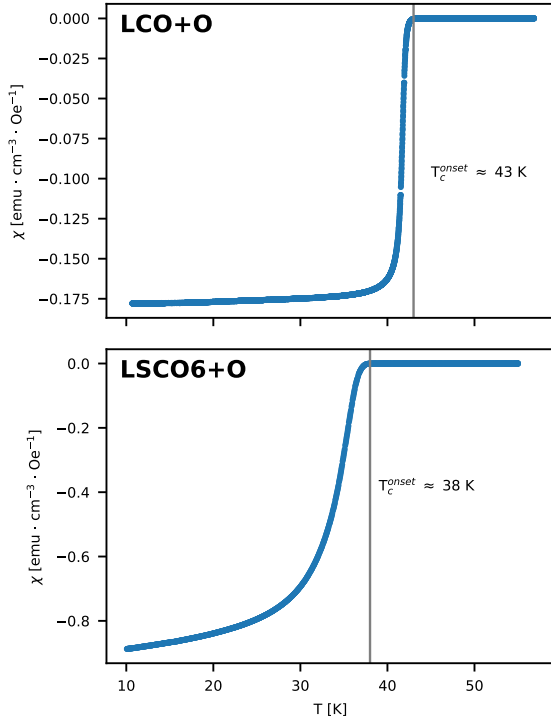


FIG. S1. Magnetic Susceptibility of both samples measured using a Vibrating Sample Magnetometer (VSM), clearly showing a superconducting transition temperature $T_c^{\text{onset}} \approx 38$ K for LCO+O and $T_c^{\text{onset}} \approx 43$ K for LSCO6+O. Data has been normalized to absolute units using the density $\rho = 7.11$ g/cm³, and a demagnetization factor of $N = 1/3$. The LCO+O Sample has previously been studied and characterized in [1].

A. Sample characterization

The samples studied are high-quality single crystal $\text{La}_2\text{CuO}_{4+\delta}$ (LCO+O) and $\text{La}_{1.94}\text{Sr}_{0.06}\text{CuO}_{4.035}$ (LSCO6+O). Both have been characterized by magnetization measurements as shown in Fig. S1, showing $T_c^{\text{onset}} \approx 43$ K (LCO+O) and $T_c^{\text{onset}} \approx 37.5$ K (LSCO6+O).

B. Phonon measurement details

For the bond-stretching phonon, it is desirable to measure in the highest achievable odd-index Brillouin Zone (BZ) [2]. We thus performed measurements in the (5,5,0) BZ in steps of 0.05 r.l.u with energies between 65 and 90 meV. To limit the spurious signal originating from the scattering plane (see SM), our sample was tilted by 12 degrees around the [1,1,0] axis, without affecting phonon measurements in the $(q,q,0)$ direction.

For measurements in magnetic fields, the sample could not be tilted and the PSD was replaced with a He³ single-detector setup in order to compensate for the decrease in intensity due to sample environment. While the spectral features of the phonon peak was partly obscured by spurious scattering, the increased counting statistics allowed us to better compare between $H = 0$ T and $H = 10$ T.

The raw data and dispersion is reported in the main text, while the linewidths are reported in Figure S2. Similar to what has been observed in LNSCO and LSCO15 [3], the linewidths correlate with the phonon softening.

C. Identification/subtraction of spurious features

Spurious features in our neutron scattering experiments were initially observed as a high number of counts in a monitor placed before the analyser at certain combinations of energy and momentum. This, in turn, contributes to the measured signal as spurious scattering. We identified this scattering as accidental Bragg scattering (A-type)[4] from the (8,4,0) Bragg reflection. Figure S3 outlines the scattering geometry responsible for accidental scattering along with a simulation of where to expect a spurious signal in our experiments. The simulation is performed with $k_f = 2.662 \text{ \AA}^{-1}$, $a = 5.34 \text{ \AA}$ and $b = 5.36 \text{ \AA}$.

As shown in Figure S3, the spurious scattering coincides with the phonon dispersion and it can be difficult to separate the signals. Using a position-sensitive detector, it is possible to separate the contributions by integrating over certain areas of the detector to avoid the spurious signal. Figure S4 illustrates the definition of these areas along with the result of the data-reduction. During the

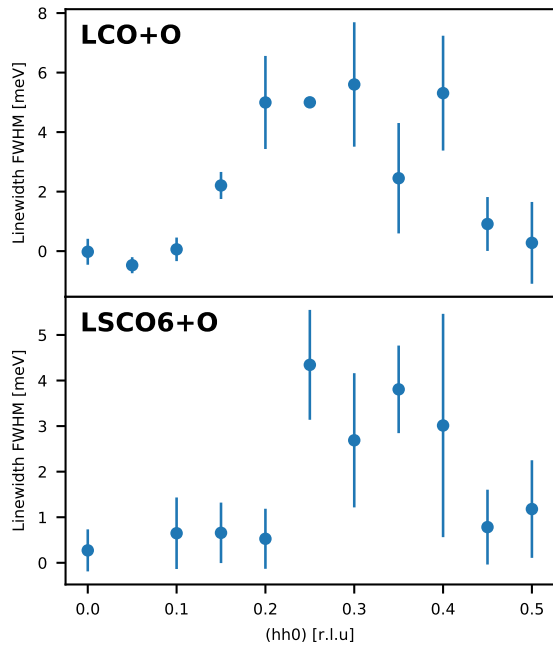


FIG. S2. Linewidths of dispersion presented in the main text (Fig. 3). The linewidths presented is only the Lorentzian (DHO) contribution. The instrumental (Gaussian) broadening was fixed to 5.4 meV (FWHM).

data-reduction, the final errorbars are normalized using the region-of-interest areas. While the spurious features are centered outside the field-of-view of the phonon, the tail of their scattering will contribute to the observed phonon intensity. For this reason, it is necessary to subtract the ‘background’-intensity.

D. Phonon calculations

Phonon calculations based on Density Functional Theory (DFT) in the fully relaxed high-temperature tetragonal (I4/mmm) crystal structure of La_2CuO_4 (LCO) were performed with the Vienna Ab-initio Simulation Package (VASP) [5–7]. Projected Augmented Wave (PAW) potentials [8] were used for all elements and the Perdew-Burke-Ernzerhof revised for solids (PBEsol) functional [9] was used for the exchange-correlation potential. Phonon calculations were performed in the finite displacement approach using the PhonoPy code [10]. We performed non-spin polarized calculations which incorrectly predict a metallic ground state of LCO. This prediction is, however, reasonably consistent with overdoped LSCO ($x = 0.23$) [11]. Phonon calculations on this metallic ground state are shown in Figure S5. We note that the metallic Cu-O bond-stretching mode is remarkably similar to our experiment in terms of absolute energies at the zone center and boundary. In addition, the sinusoidal shape of the dispersion is apparent.

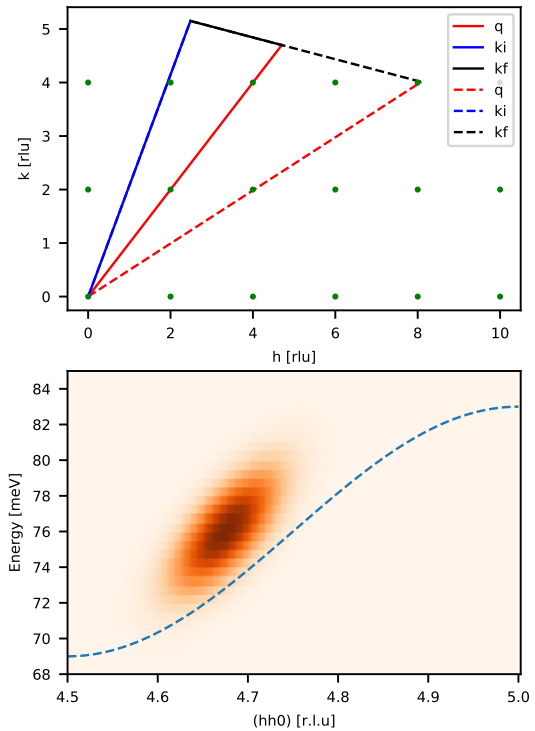


FIG. S3. **Top:** Scattering triangle responsible for the A-type spurious scattering (broken lines) at $Q = (4.7, 4.7, 0)$. Green points represent Bragg peaks in the (h, k) -plane. The $(8, 4, 0)$ Bragg reflection is responsible for the spurious scattering. **Bottom:** Simulated effect of the $(8, 4, 0)$ reflection on a Q - $\hbar\omega$ map assuming a Gaussian spurious signal depending on distances in Q . Broken line represents a ‘normal’ sinusoidal dispersion in this region.

E. Instrument Resolution

Instrument resolution was estimated using the RESTRAX software [12]. Figure S6 shows a colorplot of LSCO6+O data along with the calculated resolution ellipsoid. Since we are in the so-called focusing condition (the slope of the dispersion coincides with the slope of the resolution ellipsoid). We used the peak width at the zone center as our ‘baseline’ energy resolution in the data analysis. Our fitting is thus performed using a Voigt lineshape where the Gaussian width is fixed to $\sigma = 2.3$ meV (5.42 meV (FWHM)).

F. Anomaly amplitude and phase separation

Figure S7 shows our anomaly amplitudes from the main text (Figure 3) compared to a linear combination of the anomaly amplitude of LNSCO and LSCO15. While the numbers are chosen in an arbitrary way, the data is consistent with a picture where the oxygen-doped samples are phase separated into an insulating $x = \frac{1}{8}$ phase

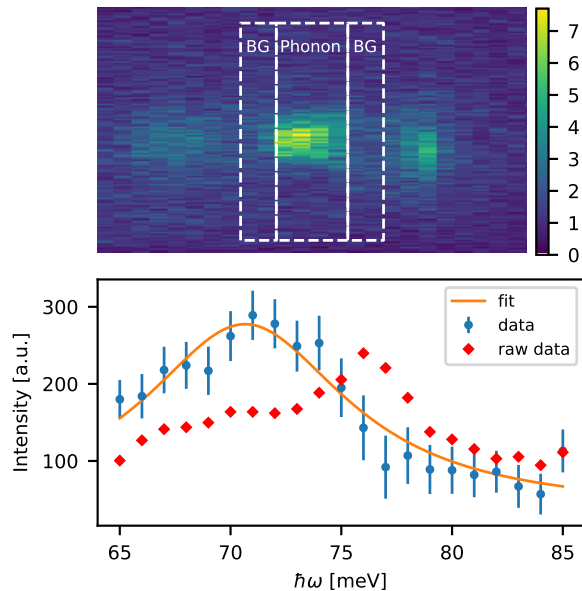


FIG. S4. Illustration of the data reduction performed using the PSD. **Top:** Summed raw data from an energy scan at $q = (4.65, 4.65, 0)$. The dashed lines denote the regions of interest (ROI) used in the data reduction. The geometry of the instrument ensures that the desired phonon scattering will occur in the ‘Phonon’ ROI. **Bottom:** Corresponding raw data (diamonds) and reduced/normalized (circles) data. The raw data is obtained by only considering the ‘Phonon’ ROI, while the reduced data is obtained by subtracting the intensity from the two ‘BG’ ROIs. The solid line is a fit to a DHO lineshape (see main text).

and a superconducting $x \approx 0.15$ phase.

-
- [1] H. Jacobsen, S. L. Holm, M.-E. Lăcătușu, A. T. Rømer, M. Bertelsen, M. Boehm, R. Toft-Petersen, J.-C. Grivel, S. B. Emery, L. Udby, B. O. Wells, and K. Lefmann, *Phys. Rev. Lett.* **120**, 037003 (2018).
- [2] R. J. McQueeney, Y. Petrov, T. Egami, M. Yethiraj, G. Shirane, and Y. Endoh, *Phys. Rev. Lett.* **82**, 628 (1999).
- [3] D. Reznik, L. Pintschovius, M. Fujita, K. Yamada, G. D. Gu, and J. M. Tranquada, *J Low Temp Phys* **147**, 353 (2007).
- [4] G. Shirane, S. M. Shapiro, and J. M. Tranquada, *Neutron Scattering with a Triple-Axis Spectrometer: Basic Techniques* (Cambridge University Press, 2002).
- [5] G. Kresse and J. Hafner, *Phys. Rev. B* **48**, 13115 (1993).
- [6] G. Kresse and J. Furthmüller, *Computational Materials Science* **6**, 15 (1996).
- [7] G. Kresse and J. Furthmüller, *Phys. Rev. B* **54**, 11169 (1996).
- [8] G. Kresse and D. Joubert, *Phys. Rev. B* **59**, 1758 (1999).
- [9] G. I. Csonka, J. P. Perdew, A. Ruzsinszky, P. H. T. Philipsen, S. Lebègue, J. Paier, O. A. Vydrov, and J. G. Ángyán, *Phys. Rev. B* **79**, 155107 (2009).
- [10] A. Togo and I. Tanaka, *Scripta Materialia* **108**, 1 (2015).
- [11] C. E. Matt, D. Sutter, A. M. Cook, Y. Sassa, M. Månsson, O. Tjernberg, L. Das, M. Horio, D. De-straz, C. G. Fatuzzo, K. Hauser, M. Shi, M. Kobayashi, V. N. Strocov, T. Schmitt, P. Dudin, M. Hoesch, S. Pyon, T. Takayama, H. Takagi, O. J. Lipscombe, S. M. Hayden, T. Kurosawa, N. Momono, M. Oda, T. Neupert, and J. Chang, *Nature Communications* **9**, 972 (2018).
- [12] J. Šaroun and J. Kulda, *Physica B: Condensed Matter Proceedings of the First European Conference on Neutron Scattering*, **234-236**, 1102 (1997).
- [13] H. E. Mohottala, B. O. Wells, J. I. Budnick, W. A. Hines, C. Niedermayer, L. Udby, C. Bernhard, A. R. Moodenbaugh, and F.-C. Chou, *Nature Materials* **5**, 377 (2006).

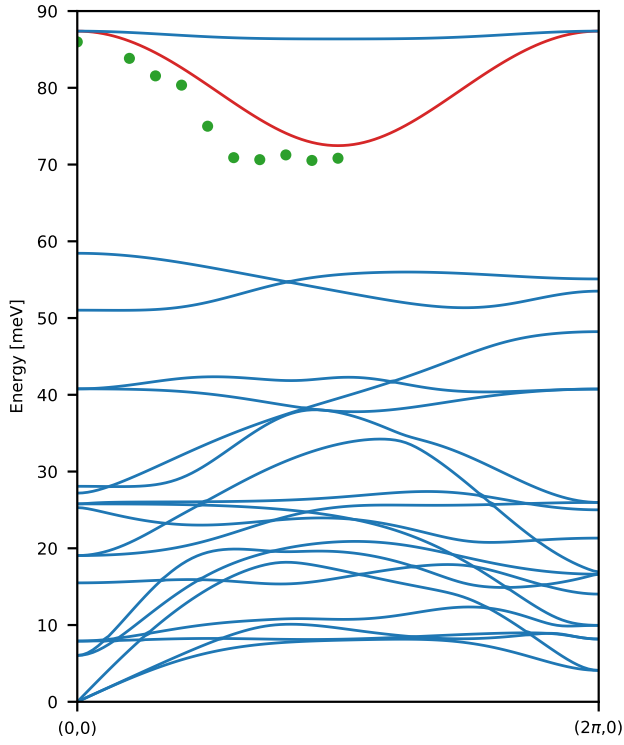


FIG. S5. Calculated phonon dispersion of La_2CuO_4 in the $(\pi, 0)$ direction of the tetragonal Brillouin Zone. The Cu-O bond-stretching mode is highlighted in red. Experimentally obtained dispersion of LSCO6+O is shown in green. Absolute energies at the boundary and center are accurate to ≈ 3 meV

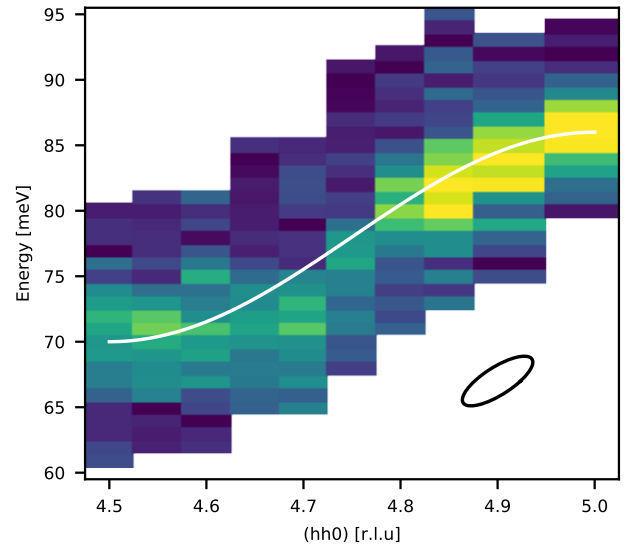


FIG. S6. Colorplot of LSCO6+O data. The black ellipsoid represents the projected resolution FWHM contour and the white line is the 'normal' sinusoidal dispersion.

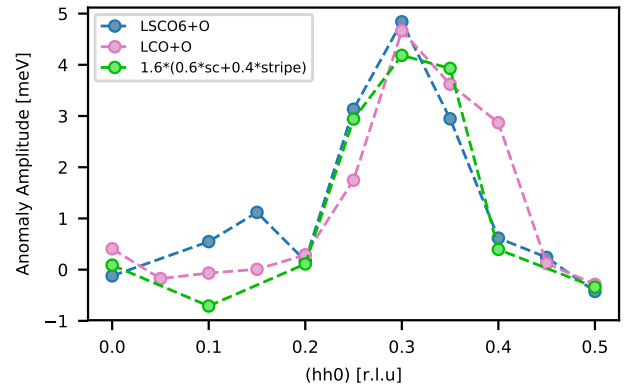


FIG. S7. Anomaly amplitude of LCO+O and LSCO6+O compared to a linear combination of stripe phase LNSCO (stripe) and optimally superconducting LSCO15 (sc). The numbers are chosen arbitrarily but correspond well to the known phase separation values from literature [13]